

## The volcanic association of Las Lomadas area, Corona Chico Volcanites. Somún Curá Magmatism. Río Negro province, Argentina

Marcela B. REMESAL, María Elena CERREDO, Pablo D. CORDENONS & Juan M. ALBITE

IGeBA (UBA-CONICET)- Departamento de Ciencias Geológicas, FCEyN, Ciudad Universitaria, CABA.  
Argentina. E-mail: mremesal@yahoo.com.ar

**Abstract:** This contribution deals with the Corona Chico Vulcanites, within the Somún Curá Magmatic Province, northern Extra-Andean Patagonia. The studied area is located to the north of the Alta Sierra de Somún Curá Volcanic Complex and is made of several basaltic volcanic buildings of varied morphologies: spatter cones, tuff ring and long lava flows related to small shield volcanoes (of *scutulium* type). Petrographic characteristics as well as whole rock chemical composition suggest a time progressive increase in alkalis content and a shift from early transitional terms to basanitic rocks in the latest stages. A simulation of the source yielded for Las Lomadas rocks an asthenospheric source in the garnet-spinel facies, with associated low partial melting percentages (< 7-8%). Within the studied rock set, the spatter cones sequence displays geochemical affinities with the basaltic component of Alta Sierra de Somún Curá Volcanic Complex.

**Key words:** Corona Chico Vulcanites, Somún Curá Magmatic Province, petrology

**Resumen:** ~~Falta título en castellano.~~ Esta contribución aporta al conocimiento de un sector de la Provincia Magmática de Somún Curá en el norte de la Patagonia Exrandina. El sector estudiado, que es parte de los afloramientos definidos como Vulcanitas Corona Chico, se extiende al Norte del Complejo Volcánico Alta Sierra de Somún Curá, y comprende una variedad morfológica de edificios volcánicos de composición basáltica: conos de salpicadura, anillos de tobos y flujos lávicos relacionados a pequeños volcanes en escudo (tipo *scutulium*), enumerados en secuencia temporal relativa. La petrografía, así como la composición química de roca total indican un progresivo aumento de la alcalinidad desde los componentes más tempranos de carácter transicional hasta los estadios finales con términos basaníticos. La simulación de la fuente mantélica modelada para las rocas estudiadas del sector de Las Lomadas indica manto astenosférico en facies de granate - espinelo con bajos porcentajes de fusión parcial (<7-8%). Dentro del conjunto estudiado, la secuencia de los conos de salpicadura muestra una afinidad geoquímica con los términos basálticos del Complejo de Alta Sierra de Somún Curá.

**Palabras clave:** Vulcanitas Corona Chico, Provincia Magmática de Somún Curá, petrología

### INTRODUCTION

This paper deals with the petrography and geochemistry of the volcanic rocks of Las Lomadas area, which is included within the Corona Chico Vulcanites (CChV) in Río Negro Province. Within the framework of the Somún Curá Magmatic Province (SCMP) in northern extra-Andean Patagonia (Figure 1a and b), two main magmatic stages were distinguished: a *plateau* stage, represented by the Oligocene-Miocene subalkaline basalts of the Somún Curá Formation and a post-*plateau* stage which includes several Miocene basalt-trachyte (rhyolite) complexes (Figure 1 b) (Corbella, 1974; Remesal, 1988; Franchi *et al.*, 2001; Kay *et al.*, 2007) and the above mentioned CChV.

The Alta Sierra de Somún Curá Volcanic Complex (ASSCVC) is the northernmost post-*plateau* assemblage set over the Somún Curá basaltic *plateau* (Figure 1b). The ASSCVC basalt to trachyte assemblage is dominated by basaltic lava flows with subordinated pyroclastic contributions located at central Río Negro Province. The ASSCVC defines a widespread subalkaline-alkaline series (Remesal *et al.* 2016a; Maro & Remesal, 2012). Geochronological information related to the trachyte facies includes K/Ar whole rock data which indicate a middle to late Miocene (~ 8-12 Ma) age for the differentiated members of the Complex (Linares 1979; Franchi *et al.*, 2001), that was recently confirmed by a  $^{206}\text{Pb}/^{238}\text{U}$  SHRIMP age of 10.47±0.31-0.47Ma (Remesal *et al.*, 2018a).

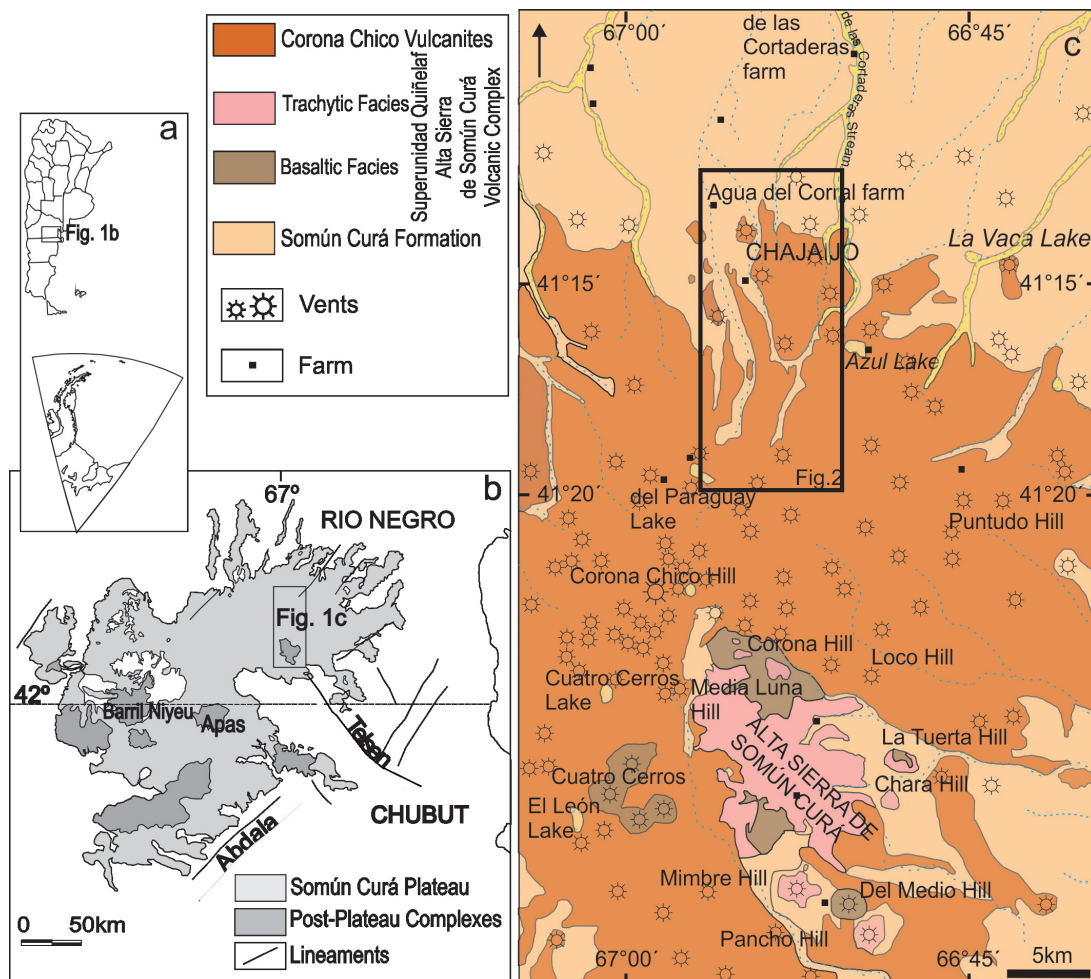


Fig. 1. a) Location map of the Somún Curá Magmatic Province in Argentine Republic; b) Sketch map of Somún Curá Magmatic Province, depicting the *plateau* extension and the *post-plateau* complexes; c) Geologic map with the extension of Alta Sierra de Somún Curá Volcanic Complex and neighboring Corona Chico Vulcanites (location in Figure 1b) with indication of the studied area. After Franchi *et al.*, 2001.

CChV represent an informal unit that embodies basic volcanic rocks outpoured over the Somún Curá *plateau*, likely belonging to several petrologic types spanning from saturated transitional basalts to basanites and foidites (Remesal *et al.*, 2017; Franchi *et al.*, 2001; Corbella 1985). CChV cover a large area that surrounds the ASSCVC (Figure 1c) and were preliminary attributed to the late Oligocene-early Pliocene realm (Franchi *et al.*, 2001). A recently published (Remesal *et al.*, 2017)  $^{87}\text{Rb}/^{86}\text{Sr}$  errorchronone built with seven samples of ASSCVC and CChV yielded  $13.8 \pm 8.3$  Ma (MSWD=1). Therefore, the CChV are provisionally assigned to the Langhian/Serravalian (Middle Miocene).

## GEOLOGIC FRAMEWORK

CChV (Franchi *et al.*, 2001) is a volcanic field composed of numerous monogenetic basaltic volcanoes (in the sense of Valentine & Connor, 2015) which encompass the hawaiian to strombolian styles of eruption. Within them, the spatter cones dominate and show variable welding degrees, relative heights between 30-100m and widths that can reach up to 1 km. These widespread volcanic buildings result from processes dominated by lava fountaining with bursts of melt spatters which accumulate around the crater and may move downwards as rootless lava flows producing long clastogenic lavas (up to 1 km long).

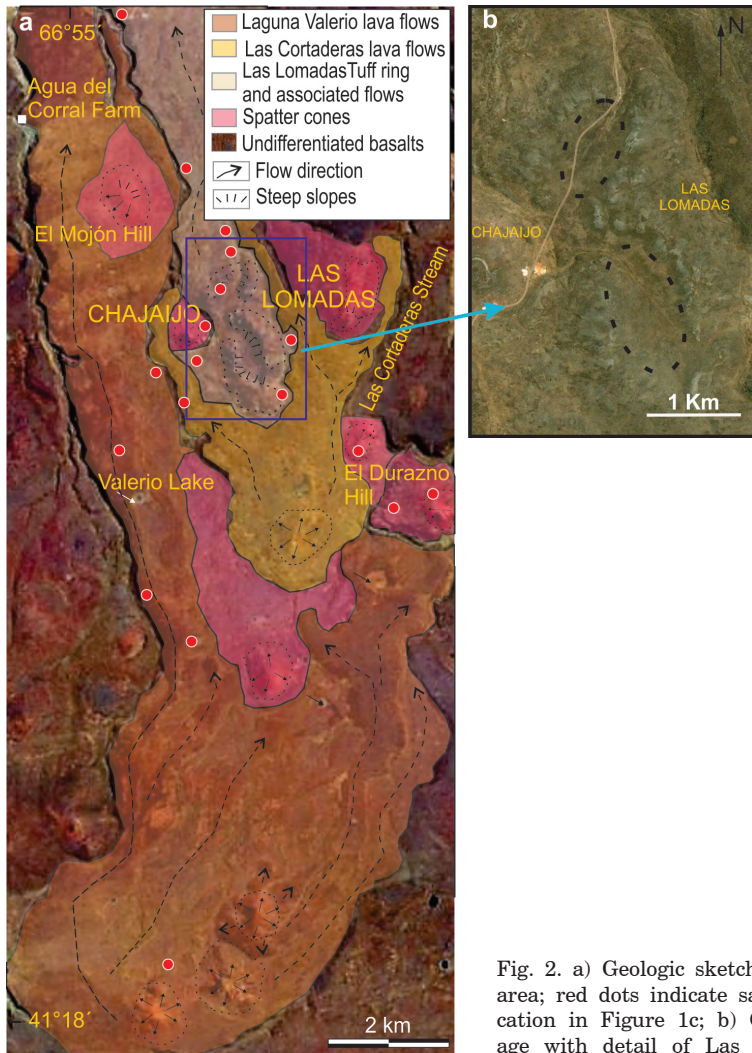


Fig. 2. a) Geologic sketch of Las Lomadas area; red dots indicate sampling sites. Location in Figure 1c; b) Google Earth image with detail of Las Lomadas craters.

CChV overlay the Somún Curá Formation (Ardolino, 1981), corresponding to the *plateau* stage, which shows continuous outcrops some 5 km north of the studied area. There, a recently published  $^{40}\text{Ar}/^{39}\text{Ar}$  age ( $21.6 \pm 0.5$  Ma, Remesal *et al.*, 2018b) indicates early Miocene times for the *plateau* stage. The immediately underlying rock units comprise variable thicknesses of the Paleocene Roca Fm. and Eocene-Oligocene Sarmiento Group exposed at Cerro Chara in the ASSCVC and in the northern *plateau* margin. Roca Fm. is made of sandstones, coquina and pelites deposited in a shallow marine to fluvio-lacustrine setting. The Sarmiento Group includes tuffaceous sandstones, tuffs and paleosols (Ardolino & Franchi, 1993). The northernmost *plateau* basalts lie in unconformity over either Roca Fm., Sarmiento

Group or the siliceous volcanic rocks of Marifil Complex (Remesal *et al.*, 2018b; Franchi *et al.*, 2001 and references therein).

This contribution is devoted to a restricted sector of the CChV; we focus on Las Lomadas area, located to the north of the ASSCVC (Figure 1c) and mostly composed of basaltic lavas with subordinated pyroclastic component. Las Lomadas area (Figure 2) includes several emission centers with distinct characteristics. The volcanic buildings are monogenetic and < 100 m height, associated with hawaiian to strombolian eruptions, producing spatter cones, scoria ramps of coarse brecciated textures. Variations in the degree of welding result in interlayering of pyroclastic banks with levels of clastogenic lavas. Small shield volcanoes of *scutulum* type

and elliptical tuff rings are also found within the studied area.

#### LAS LOMADAS AREA

In Las Lomadas area the landscape is dominated by basaltic lavas with subordinated pyroclastic products in an apparent monotonous sequence. Nevertheless, close inspection reveals a more complex structure composed of several volcanic landforms. The most outstanding corresponds to a central shallow ellipsoidal crater surrounded by a tuff ring: Las Lomadas (LLtr). This central structure is in fact composed of two associated ellipses: a larger one of NS oriented major axis and the other with a NNE-striking major axis (Figure 2b). Several spatter cones flank LLtr: El Mojón and Chajaijó (Csc) at the West and El Durazno spatter cone (EDsc) at the East (Figure 2 a). Other two unnamed spatter cones are included within the studied area. To the south, another emission center is associated with long lava lobes which flowed northwards enveloping the above-mentioned volcanic morphologies. This landform, which in map view draws a horseshoe pattern, is hereinafter designed as Las Cortaderas (LC). It is in turn surrounded by other northward directed flows: The Laguna Valerio (LV), with several emission centers located further south (Figure 2 a). All share a common morphology of low aspect ratio and shallow relief.

Mutual crosscutting relationships among the products of each volcanic center is suggestive of the following temporal evolution:

\*spatter cones

\*explosive deposits resulting in Las Lomadas tuff rings and associated lava flows

\*single or multiple centers associated with large lava flows

- Las Cortaderas

- Laguna Valerio

The description is ordered according to the interpreted time sequence:

#### Spatter cones

**Chajaijó spatter cone (Chsc):** This apparatus shows a sequence characterized by basal and top red levels made of agglutinated bombs with interlayered welded flows of clastogenic lavas. Overall, the edifice displays a banded structure at the large scale. Morphologic and stratigraphic evidences suggest that Chsc is one of the oldest emission centers of the studied area.

Clastogenic lavas are banded and brecciated

(with eutaxitic texture, Figure 3a), porphyric with olivine microphenocrysts with Low Temperature Iddingsite (LTI), and larger light brown clinopyroxene, plagioclase and orthopyroxene crystals displaying variable degrees of disequilibrium. Green clinopyroxene crystals are generally of rounded shapes or low-aspect ratio prisms, with thin spongy rims. Plagioclase (andesine?) is subtabular with rounded corners and thin reabsorbed borders. Exceptionally some plagioclase crystals show kinked twin planes. Orthopyroxene enveloped by coronae of clinopyroxene-olivine-phlogopite intergrowths complete the crystal assemblage (Figure 3b).

In addition, gabbroic enclaves, pyroxene glomerocrysts and quartz xenocrysts strengthen the porphyritic character of these rocks. The cm-scale gabbroic enclaves (Figure 3c) of irregular outlines and diabasic texture are made of labradorite and clinopyroxene; other mafic enclaves are characterized by fan-shaped subgrains in clinopyroxene and combed twins in plagioclase. Small quartz xenocrysts, showing subgrains, are rimmed by tiny pyroxene needles.

The groundmass is usually banded, dominated by oriented plagioclase microliths accompanied by olivine, clinopyroxene, opaque minerals and phlogopite.

**El Durazno spatter cone (EDsc)** comprises red bomb deposits and reddish to grayish porphyritic basaltic lavas at the top. Clastogenic basaltic lavas are porphyric with olivine microphenocrysts of around 0.3 mm showing high temperature iddingsite (HTI), accompanied by a set of crystals displaying variable degrees of disequilibrium: rounded crystals of clinopyroxene and plagioclase (around 1-2 mm); plagioclase often show sieve-textured cores, in other cases subgrains; orthopyroxene rimmed by a thin ring either of olivine or olivine-clinopyroxene. In addition, quartz (enveloped by tiny clinopyroxene prisms, Figure 3d) and zircon xenocrysts (Figure 3e) reinforce the porphyritic character of the lava. The groundmass is fine grained, dominated by fluidal (oriented?) plagioclase microliths and olivine, with lesser and smaller clinopyroxene and opaque minerals. Irregular amygdaloids show a fine-grained aggregate of silica in radial arrangement.

The groundmass, both in Chsc as in EDsc, is usually banded, dominated by oriented plagioclase microliths accompanied by olivine, clinopyroxene, opaque minerals and phlogopite (Figure 3f).

Clastogenic lavas are characterized by eutaxitic textures which are identified both at the

outcrop scale as under the microscope, with interlayering of reddish and dark grey fiammes. Evidences of reomorphism in the pyroclastic material are indicated by the internal structures and surfaces of these flows which are interpreted as clastogenic lava flows (after Cas and Wright, 1987; Summer, 1998).

Most of the plagioclase crystals within these flows are mechanically broken, with rupture surfaces which crosscut crystal compositional zoning, or bound with vesicle walls, suggesting that gas burst was the agent of crystal breaking (Figure 3g). Some of the feldspar crystals showing a progressive grain size decreasing to the groundmass, seem to be broken fragments. All these evidences point to the clastogenic nature of the flows.

### **Tuff ring**

**Las Lomadas center (LLtr):** This ellipsoidal crater, is roughly N-S oriented, (Fig. 2 a, b) and represents the most prominent relief within the studied area. It is provisionally interpreted as a tuff ring composed of two assembled ovals (with major and minor axes of 1.4-0.6 km and 0.4-0.65 km respectively, measured from the crest of the tephra ring) and a few tens of meters deep (20-40m, measured also from the crest of the tephra ring). Gentle external slopes (angle  $\sim 10^\circ$ ) contrast with steep internal walls. Both rings may be related to synchronous explosions, resulting from the magma interaction with either surficial or subsurficial water.

The pyroclastic deposits around the ring grade from basal coarse ash to upper agglomerate consisting of medium to coarse lapilli; these deposits extend as far as 3 km from the ring. The ash deposits were mostly reworked by fluvial processes.

The associated pyroclastic products of LLtr comprise red agglomerates, lapillites and tuffs, and locally host vegetal remains. Lapilli particles are generally oxidized, with rare plagioclase and rounded orthopyroxene inclusions. Ash particles are varied: feldspars, volcanic fragments and some glass shard ghosts.

At least some part of the pyroclastic deposits resulted from diluted pyroclastic density surges which produced non welded monomictic lithic breccias rich in glass shards, ash sized matrix and widespread palagonitized glass. The subordinated but significant presence of glass shard of blocky morphology along with the generalized palagonite replacement witness the magma/water interaction process.

The fallout deposit bears a coarse granulometric fraction made of juvenile fragments up to 1 cm, corresponding to totally oxidized glass (tachyllite) of vitrophyric texture (plagioclase microliths and rare orthopyroxene and plagioclase phenocrysts set in an opaque groundmass) (Figure 3l). The glass fragments show even outlines and are vesicle rich. The fine grained matrix (lapilli-ash) is made of juvenile fragments, rounded volcanic clasts (0.6-0.8 mm) of fluidal texture, brown glass with some crystals, blocky glass fragments (0.2-0.3mm) and crystal fragments (plagioclase and rare reddish amphibole). Yellowish sideromelane, partially pallagonitized is found at interstitial locations. (Figure 3 m, n, o)

Two short lava flows were sampled likely postdating the explosive stage, one at the western ring flank, and one at the eastern flank.

The western lava flow is vesicle rich, with some amygdala filled with carbonate and clay minerals (with relic grains of plagioclase, volcanic fragments, oxidized mafic minerals). Rocks are mildly porphyric, with olivine (around 1.5 mm, displaying LTI) and clinopyroxene (around 0.5 mm) microphenocrysts. Clinopyroxene often shows somewhat spongy rims. Reabsorbed plagioclase crystals, orthopyroxene with olivine-clinopyroxene coronae, rounded apatite crystals and tiny clinopyroxene glomerocrysts are outstanding. The groundmass is made of oriented plagioclase laths and isometric tiny crystals of olivine, pyroxene and opaque minerals. Locally some small pockets of oxidized glass are found hosting posthumous plagioclase needles.

The lava flow on the Eastern side of Las Lomadas comprise clastogenic lavas, porphyric with clinopyroxene and olivine microphenocrysts showing LTI. In addition, orthopyroxene crystals enveloped by clinopyroxene-olivine rims and relic reabsorbed spongy plagioclase highlight the porphyric character. The groundmass is very fine grained, composed of plagioclase, clinopyroxene, opaque minerals and olivine in a mesostasis likely made of feldespatoïd (analcime?). This lava bears also rounded gabbroic enclaves composed of plagioclase and orthopyroxene (showing olivine-spinel coronas) with evidences of deformation (subgrains in pyroxene, some local recrystallization in plagioclase).

### **Large lava flows**

**Las Cortaderas center (LCc):** This very low aspect/ratio apparatus (h/r:0.03) is associated with very long basaltic lava flows ( $\sim 5-7$  km), which surround the previously described volcanic facies.

The map outline of these lavas was likely constrained by the older positive volcanic landforms, some of which have been already described and others, probably made of loose material, are presently partially eroded.

The emission center of these basalts is of low relief (30-40 m), nearly circular in map view (diameter around 3 km). This monogenetic building shows the characteristic profile of a shield volcano, with a slope of around 3°. Given the reduced size and the low volume (~ 0.5 km<sup>3</sup>), this apparatus is classified as *scutulum* (in the sense of Noe-Nygaard, 1968 and Walker, 2000).

Two major lava lobes flowed northwards following the regional slope, as far as 6 km from the emission center. A significant change in the surface texture of the lava flows is related to the palaeo-relief slope. The flows in the subcircular sector and low slope show hummocky morphologies characteristic of the pahoehoe lavas, with ridges near to slope breaks in the margins of the *scutulum* structure. The north-directed, thin lobes, in turn, show a soft surface suggesting lobe rupture and the creation of a new tube toward the steepest slope. These changes in the surface texture indicate the propagation of lava lobes which protrude and inflate, according to the palaeo-relief.

The more proximal flows are porphyric, rich in clinopyroxene and olivine phenocrysts, (Figure 3h) the former are either colorless or green and often show sieve-textured cores; the latter display LTI thin rims. In addition, rounded clinopyroxene and plagioclase with disequilibrium features are also recognized. The medium grained groundmass is made of plagioclase and clinopyroxene, and lesser olivine and opaque minerals;

locally there are pockets of feldspars.

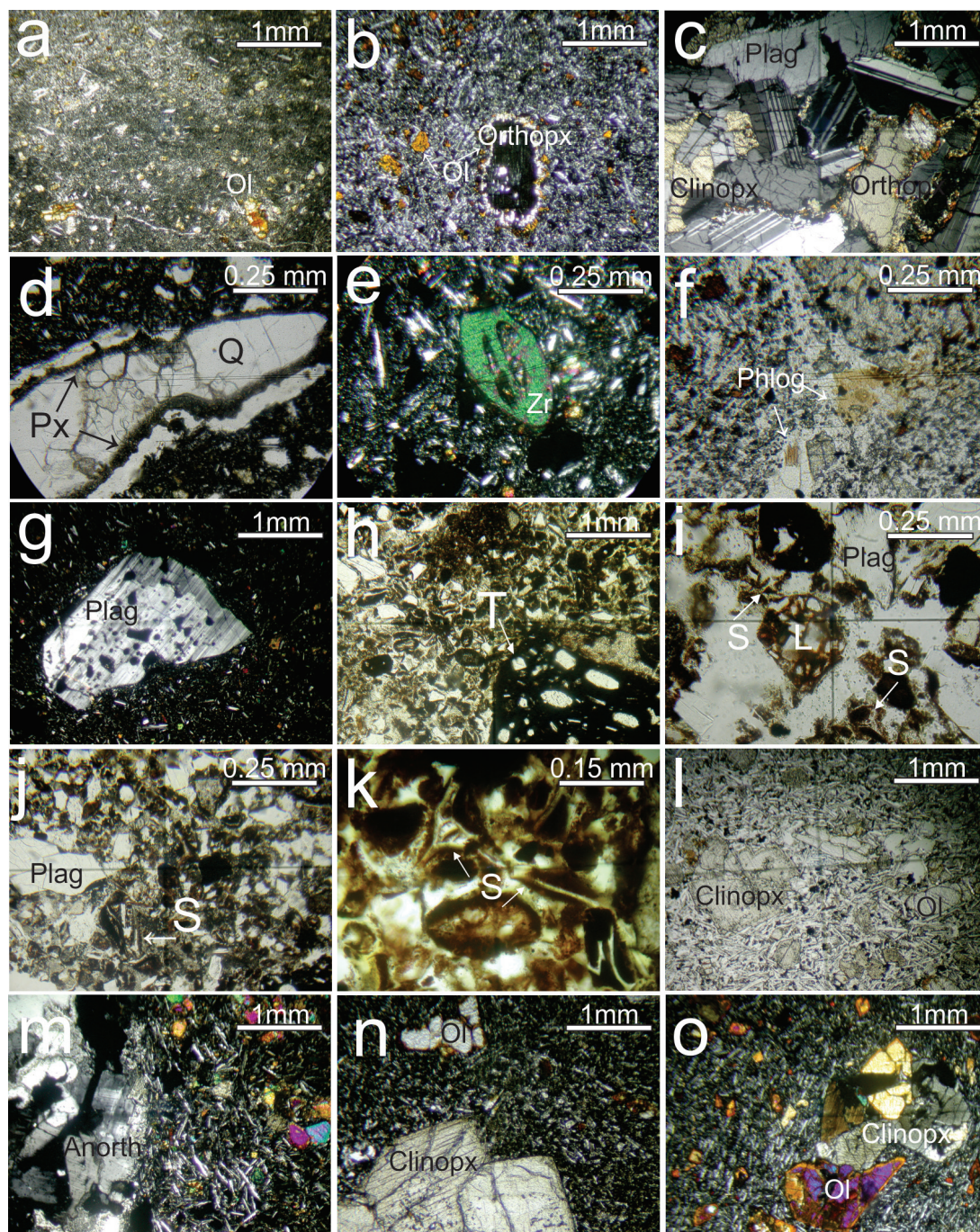
The most distal flows bear a phenocryst assemblage like the above described; colored apatite occurs as a microphenocryst phase accompanied by green clinopyroxene glomerocrysts with opaque-pyroxene symplectite intergrowth cores. A grain size transition from olivine and clinopyroxene microphenocrysts to groundmass microliths is appreciated, accompanied by tiny plagioclase laths. A mesostasis devitrified to feldspar and pyroxene needles is locally observed.

This facies bears centimeter-scale enclaves of leuco-trachyte composition, made of a medium grained (0.5-1.5 mm average grain size) plagioclase-anorthoclase aggregate (Figure 3i).

**Laguna Valerio multicenter (LVmc):** This very low aspect/ratio landform (h/r:0.028) is the youngest within the studied area. It is associated with the longest basaltic lava flows (~ 15-20 km), which surround the previously described volcanic constructions. LV was outpoured from three emission centers which constitute in whole a low relief association with a diameter of ~ 4.5 km and a maximum relative height of ~ 65 m.

Lavas are porphyric with plagioclase-clinopyroxene enclaves of ~ 1cm, clinopyroxene glomerocrysts (made of light brown, euhedral, zonal crystals with sieve-textured cores) (Figure 3j), clinopyroxene-olivine glomerocrysts (Figure 3k), tiny relic orthopyroxene with olivine coronae, small rounded plagioclase crystals; phenocrysts correspond to clinopyroxene and olivine (2-2.5mm, with LTI, some of skeletal habit), generally accompanied by green clinopyroxene microphenocrysts. The groundmass may be either very fine grained made of plagioclase microliths

Fig. 3 (next page). a) Clastogenic lava of Chajaijé spatter cone, showing eutaxitic texture and olivine microphenocrysts with LTI. Plane polarized light; b) Clastogenic lava of Chajaijé spatter cone with orthopyroxene rimmed by a corona of clinopyroxene-olivine-phlogopite intergrowth. Strongly iddingsitized olivine. Crossed polars; c) Gabbroic enclave in Chajaijé spatter cone displaying diabasic texture with labradorite, orthopyroxene (with olivine-clinopyroxene rim) and clinopyroxene. Crossed polars; d) Clastogenic basaltic lava of El Durazno spatter cone bearing quartz xenocrysts enveloped by tiny clinopyroxene prisms. Plane polarized light; e) Rounded zircon xenocryst in clastogenic lava of El Durazno spatter cone. Crossed polars; f) Typical groundmass of spatter cones is usually banded, dominated by oriented plagioclase microliths accompanied by olivine, clinopyroxene, opaque minerals and phlogopite. Plane polarized light; g) Clastogenic lava of El Durazno spatter cone: mechanically broken plagioclase. Crossed polars; h) Porphyric lava of Las Cortaderas, with clinopyroxene (sieved core) and olivine (with LTI) phenocrysts. Plane polarized light; i) Las Cortaderas lava with enclave of medium-grained leuco-trachyte composition, made of plagioclase-anorthoclase aggregate. Crossed polars; j) Porphyric Laguna Valerio lavas with clinopyroxene and olivine (with LTI) phenocrysts set in a very fine-grained groundmass made of a network of plagioclase laths, olivine, clinopyroxene and opaque minerals; k) Laguna Valerio lava, with a clinopyroxene (zonal)-olivine (with LTI) glomerocryst. Crossed polars; l to o) Diluted pyroclastic density current deposit of Tr structure: l) porphyric opaque tachyllite clast (basaltic glass), reddish or dark brown due to intense iron oxidation. Its presence indicates sudden cooling. Plane polarized light; m, n) blocky glass shards (S), plagioclase (Plag) and lithic, (L) clasts set in a palagonite matrix. Plane polarized light; o) detail of palagonitized matrix tuff with blocky glass shards. Plane polarized light.



> clinopyroxene > olivine > opaque minerals or a network of plagioclase laths, olivine, clinopyroxene and opaque minerals. Locally some mesostasis patches likely resulting from devitrification are made of alkaline feldspar (?) or feldspatoids (?) including needles of clinopyroxene

and opaque minerals.

#### GEOCHEMISTRY

Chemically analyzed samples from the Las Lomadas area (Table 1) are metaluminous

Table 1: Whole rock chemical data of Las Lomadas area.

	Chajaijo Sc	El Durazno Sc	Las Lomadas Tr	Las Cortaderas lv			Laguna Valerio lv
	<i>rn8</i>	<i>cn-506</i>	<i>cn 504</i>	<i>rn160</i>	<i>rn11</i>	<i>cn-503</i>	<i>cn-513</i>
SiO <sub>2</sub>	51.27	50.97	45.37	51.24	48.85	49.52	46.94
Al <sub>2</sub> O <sub>3</sub>	15.07	14.91	14.40	15.63	17.90	14.91	13.39
Fe <sub>2</sub> O <sub>3T</sub>	9.75	11.29	12.11	8.64	6.89	9.81	10.09
MnO	0.14	0.14	0.16	0.12	0.10	0.14	0.16
MgO	6.08	6.06	7.57	5.97	6.05	6.33	8.44
CaO	7.39	7.76	9.26	6.98	7.27	7.28	8.97
Na <sub>2</sub> O	3.96	3.89	4.26	4.33	3.54	4.65	4.25
K <sub>2</sub> O	1.78	1.33	1.02	2.88	2.51	3.02	2.28
TiO <sub>2</sub>	2.16	2.09	2.38	2.17	2.58	2.36	2.98
P <sub>2</sub> O <sub>5</sub>	0.57	0.53	0.83	0.57	1.08	0.81	0.86
LOI	0.42	0.43	2.10	0.48	0.6	0.12	-0.26
Total	98.59	99.40	99.51	99.01	97.37	98.94	98.09
V	197	198.14	232			195	212
Cr	179	162.09	219		310	170	239
Co	40	48.89	44.6		53	38	47
Ni	136	311.99	153		150	113	172
Rb	43	26.90	23.1		11	76.70	51
Sr	729	713.95	1064.3		620	1080	1130
Y	21	25.61	19.8			24.31	27
Zr	185	128.37	216.4			291.18	262
Nb	35.0	23.78	61.2			58.09	64.1
Ba	750	630.86	1069			1070	702
La	34.20	25.79	52			60.10	55.90
Ce	57.60	53.52	99.7			111.53	108.00
Pr	6.86	6.58	10.51			12.20	12.00
Nd	29.20	31.17	41			50.31	54.60
Sm	6.90	6.86	6.66			8.72	9.76
Eu	2.36	2.55	2.19			3.10	3.43
Gd	6.00	6.84	6.13			8.06	8.76
Tb	0.90	0.99	0.84			1.06	1.21
Dy	4.70	5.28	4.29			5.23	6.19
Ho	0.80	0.99	0.7			0.93	1.05
Er	2.00	2.51	1.94			2.40	2.52
Tm	0.27	0.32	0.25			0.28	0.29
Yb	1.70	1.96	1.54			1.75	1.79
Lu	0.24	0.29	0.21			0.23	0.22
<b>Σ REE</b>	<b>153.73</b>	<b>145.64</b>	<b>227.96</b>			<b>265.90</b>	<b>265.72</b>
Hf	4.20	2.61	5.2			5.10	4.80
Ta	2.50	1.21	3.8			3.64	3.94
Th	3.50	2.59	6			6.18	5.45
U	0.80	0.57	1.4			1.57	1.29

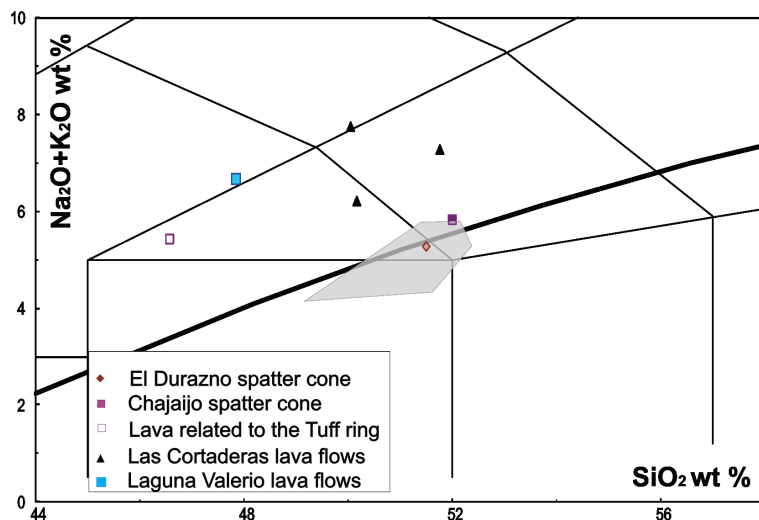


Fig. 4. Total alkalis vs.  $\text{SiO}_2$  classification diagram (Le Bas *et al.*, 1986) for the Las Lomadas rocks. Thick black line indicates the boundary between alkaline and sub-alkaline fields according to Irvine and Baragar (1971). Grey shaded area represents the compositions of basic rocks of Cerro Corona and Cerro Loco of ASSCVC (data from Maro and Remesal, 2012; Corbella, 1985).

basanites, trachybasalts to basaltic trachyandesites; the latter two may be either of transitional character or truly alkaline in the TAS diagram (Figure 4). The transitional samples belong to the spatter cones, the lava flow related to the tuff ring is a hawaiite (trachybasalt), the LC lavas are shoshonites to K-trachybasalts, whereas the youngest LV lavas are basanites.

Within the interpreted temporal schema there is progressive time shift from transitional alkaline/subalkaline terms towards alkaline rocks. Nearly the same holds for the potassium content. In the  $\text{K}_2\text{O}$  vs.  $\text{SiO}_2$  portrayal the studied rocks straddle the fields of the calcalkaline series (EDsc), the high-K calc-alkaline series (the high K-basalts of Chsc and LLtr) for the rocks of the spatter cones and the tuff ring; whereas, samples of the Las Cortaderas and Laguna Valerio lava flows plot in the alkaline shoshonite series (absarokites).

The analyzed samples from the spatter cones are transitional in the TAS diagram, these hawaiites and mugearites are *hypersthene* (9-11 %) and *olivine* (~6 %) normative. In turn, the hawaiites of Las Lomadas tuff ring have around 8% of normative *nepheline* and no modal feldspatoids, plus *olivine* (15%) and *diopside* (20%). The shoshonite lavas of the Las Cortaderas are undersaturated with normative *nepheline* (3-8%), *diopside* (13-16%) and *olivine* (10-11%); the basanite lavas of Laguna Valerio are undersaturated with normative *nepheline* (~10%), *diopside* (~22%) and *olivine* (~12%). Therefore, a temporal trend from saturated to undersaturated lavas may be inferred.

Rocks span from 57 to 68 in Mg# along with a 45-51  $\text{SiO}_2$  weight % range. Magnesium number

shows a progressive increase from the samples of the spatter cones and the tuff ring structure (57-62) to the Las Cortaderas and Laguna Valerio (63-68). LC lavas show a narrow  $\text{SiO}_2$  range (49-51%), the same holds for the spatter cones (51%).

Considering the complete available data set, rocks display well-defined negative trends against Mg# for Fe, Mn, Si and Ca, and positive relationships for P, Ti, Al. The samples related to the Tr structure and Laguna Valerio plot out of trends for Fe, Si and Ca. A scattered roughly negative trend for  $\text{Na}_2\text{O}$ , and a highly scattered correlation for  $\text{K}_2\text{O}$ . There is a time progressive trend of decreasing silica as Mg# and alkalis content increase. (Figure 5).

Significant variations in both HFS and LIL element contents are observed at almost constant  $\text{SiO}_2$ , with a clear overlap between undersaturated samples in primitive mantle (PM) multi-element pattern (Figure 6) that show marked enrichments among selected LILE and HFSE (Hf, Ti), with all the samples showing variable Ba and Sr spikes, and also positive anomalies in K except for the sample related to the Tr structure and LV lava. Other LILE (Th-U) are invariably troughs.

The chemical data set is characterized by variable degrees of enrichment in fluid-mobile elements such as Rb, Ba, and a relative Th -U depletion when compared to average OIB (Sun and McDonough, 1989). The enrichment in LILE relative to HFSE (e.g., Nb and Ta) is usually attributed to subduction-related metasomatism, because of HFSE are mostly retained in the subducted slab during its progressive dehydration, whereas LILE and LREE migrate upward in slab-derived fluids or melts and then modify

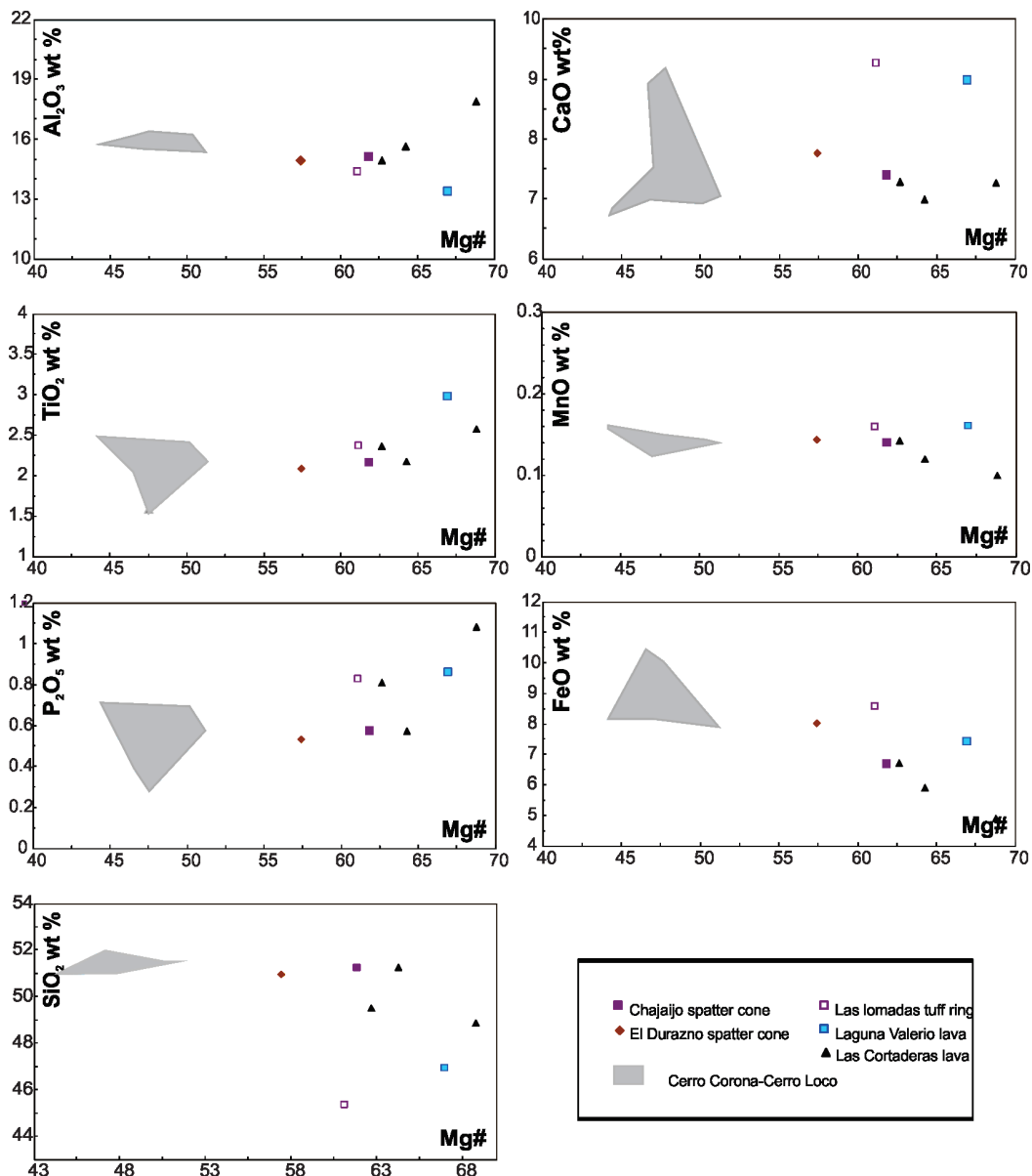


Fig. 5. Variation of major elements (wt.%) vs. Mg# in the Las Lomadas rocks. The field of the Cerro Corona and Cerro Loco (ASSCVC) basalts is also shown (data sources as in Fig. 4).

the overlying mantle wedge composition (e.g., Tatsumi, 1989).

Trace element ratios (e.g., LILE/LREE, LILE/HFSE) Nb/Yb vs. Ba/Nb may be used to discriminate between aqueous fluids and silicate melts (Figure 7). Ba easily migrates in aqueous fluids, whereas Nb and Yb are considered fluid-immobile. The marked increase in Ba/Nb ratios is paralleled by Nb/Yb variations suggesting the coupled effects of fluids as metasomatising

agents and variable degrees of partial melting.

Chondrite-normalized REE contents increase as rocks became more alkali-rich (i.e. from La/Yb ~ 10 for the EDsc to ~24 for the LC).

## DISCUSSION

Strombolian and hawaiian-style eruptions in Las Lomadas area produced low aspect ratio volcanic constructions with associated thin lava

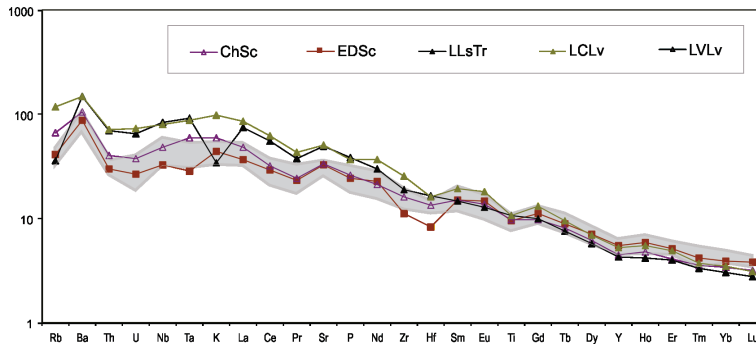


Fig. 6. Primitive mantle normalized multi-element plot for the studied rocks. Grey shaded area represents the basaltic rocks of Cerro Corona (of the ASSCVC, data from Maro and Remesal, 2012). Normalization values are from McDonough and Sun (1989).

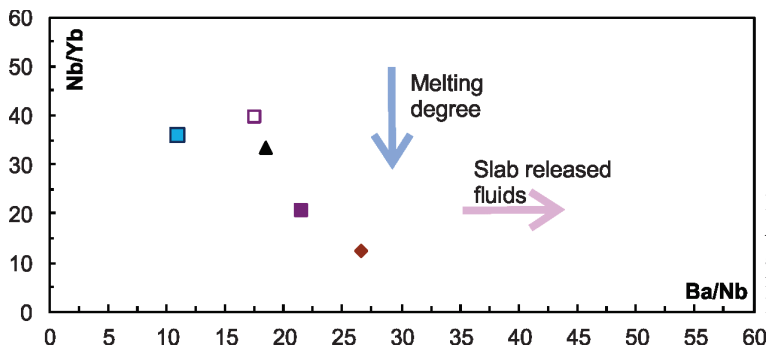


Fig. 7. Nb/Yb vs Ba/Nb diagram. Arrows represent increasing degrees of partial melting and fluid release by the slab. Symbols as in Fig. 4

flows and several spatter cones which group geographically in two main directions. The overall arrangement of the emission centers within the studied area suggests that their emplacement was controlled by NE-SW and SE-NW oriented structures. Several regional lineaments of the same orientations have been reported for North Patagonia and were related to volcanoes locations (Remesal *et al.*, 2011; Figure 1b). Moreover, NE-SW and SE-NW regional lineaments have been long recognized in the southern outcrops of the Marifil Complex (Chubut province), i.e.: Abdala and Telsen lineaments (Franchi *et al.*, 1977; Lapido & Page, 1979; Cortés, 1987; Ardolino & Franchi, 1996; Ciccirelli 1990).

Low-silica basanite, alkali trachybasalt and transitional trachybasalt to basaltic-trachyandesite lava flows, spatter cones and tuff ring make up the Las Lomadas area within the Miocene Corona Chico Vulcanites in the Somún Curá Magmatic Province.

The interpreted Las Lomadas tuff ring would have been formed when magma raised through the feeder dyke and, close to the surface, interacted explosively with groundwater. In this connection, it is important to remark that before extensive volcanic activity in SCMP, the area was the scenario of **wide plains with pastures and lagoons** cut across by numerous rivers (Ardolino *et*

*al.*, 2008).

We interpret that the spatter cones, agglomerated ramps, tephra deposits and associated lavas were produced by effusive or explosive processes (Amin & Valentine, 2017) related to typical explosive style (i.e.: strombolian-hawaiian to strombolian up to violent strombolian, given variable fragmentation degrees, Valentine and Gregg, 2008).

The presence of mafic and felsic enclaves in the mafic lavas of ASSCVC has been already reported and interpreted as a likely evidence of more or less synchronous volcanic and plutonic activity of an overall single system (Cerrodo & Remesal, 2001). The existence of epizonal differentiated mesosiliceous terms might be interpreted from the leucotrachyte enclaves hosted in the LC. Further, this could increase the trachyte component of the ASSCVC and CChV, thus enlarging the trachyte/basalt ratio of the youngest association of the SCMP.

The rare but significant presence of quartz and zircon xenocrystals in the spatter cones lavas point to the incorporation of upper-crustal materials in route to the surface. In this context, it is important to recall that Paleogene, Cambrian and Proterozoic inherited zircons have been reported for the trachyte/rhyolitic facies Agua de la Piedra Volcanic Complex (Salani *et al.*, 2019).

Petrographic observation of volcanic samples revealed disequilibrium textures, such as sieved, patchy and corroded textures in plagioclase coexisting with rounded and embayed clinopyroxene. In addition, the common presence of orthopyroxene armored within either a rim or a well-developed olivine-clinopyroxene intergrowth, also point to the hybrid nature of the magmatic liquids. These orthopyroxene textures have also been reported for the transitional and alkaline basic rocks of ASSCVC (Remesal *et al.*, 2016b). These features were reproduced experimentally and characterized as reaction zones resulting from low pressure reaction of orthopyroxene with Si undersaturated alkaline melts (Shaw *et al.*, 1998; Shaw 1999).

The possible interaction between two liquids of different composition in the studied area is also suggested by the coexistence of *q*-normative, *ol-hy*-normative and *ne*-normative rocks within a restricted area.

Although, some partially reabsorbed plagioclase crystals are often observed, the geochemical data suggest that feldspar plays no significant role in the differentiation of the studied rocks.

Low-silica basanite, hawaiiite, mugearite and shoshonite magmas ( $\text{SiO}_2$  range: 45-51 wt %) have primitive chemistry (high MgO -6-8%, magnesium numbers, and high concentrations of compatible elements) and probably rose rapidly enough from their site of partial melting to the surface to escape significant crustal contamination.

On the basis of their chemical composition, only the basalts of the spatter cones are comparable to already published data of basic rocks of the ASSCVC (Figs. 4, 6). Major element data of Cerro Corona and Cerro Loco (Corbella, 1985; Maro & Remesal, 2012) display a subalkaline-alkaline transitional trend which includes our data of the spatter cones.

#### Source of melting depth, melting percentage

The variable but high  $\text{La/Yb}_n$  slopes ( $\sim 9.5$  to 25) suggest that garnet may be a reliable residual phase. Therefore, a not very shallow mantle source may be envisaged for the magmas that gave rise to the studied rocks. To test this hypothesis, we modelled the non-modal partial melting of a spinel peridotite, a garnet peridotite and a spinel-garnet peridotite mantle source, (Table 2, Figure 8).

Table 2: Partial melting modelling parameters starting from a primitive mantle source (PM of McDonough and Frey, 1989), partition coefficients after McKenzie and O'Nions, 1991.

	Garnet- herzolite (Walter, 1998)	Spinel- herzolite (Kinzler, 1997)
<b>Mineral mode</b>		
Olivine	60	58
Orthopyroxene	21	27
Clinopyroxene	8	12
Garnet	12	
Spinel		3
<b>Melt mode</b>		
Olivine	5	10
Orthopyroxene	20	27
Clinopyroxene	30	50
Garnet	45	
Spinel		13

The analyzed samples show two distinct groups:

\*a vertical pattern is drawn by the samples of the spatter cones along with the lava related to the tuff ring structure. This trend may be the prosecution of the one described by the Cerro Corona basalts. A roughly parallel pattern is also described by neighboring complexes (Barril Niyeu and Apas, Figure 1b) pointing to sources located at variable depths.

\*In turn the long lava flows (Las Cortaderas and Laguna Valerio) plot along a single compositional trend (*i.e.* 60 *sp*- 40 *grt*) following the evolution line for a spinel-garnet bearing peridotite source.

According to this model, the partial melting degree could have spanned from 3-5 to 7-8 %. However, magma evolution process could have lead to some overestimate, therefore the results are considered as maximum values.

The systematic increase in  $\text{La/Yb}_n$  ( $\sim 9.5$  to 25) ratios displayed from transitional basaltic andesites/trachyandesitic basalts to basanites is consistent with decreasing degrees of partial melting, which is also indicated by the increasing  $\text{REE}_t$  contents from  $\sim 150$  to  $\sim 270$  ppm, and the  $\text{Yb vs Dy/Yb}$  plot.

For further support of the source depth, an artificial data-set was produced by normalizing all major element compositions to 15% MgO by fractional addition of olivine, in order to avoid

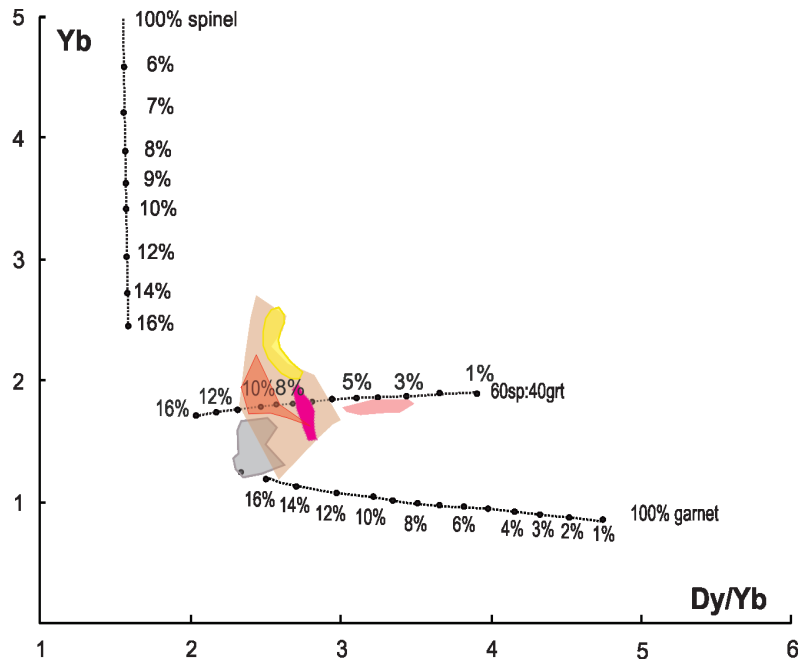


Fig. 8. Yb vs. Dy/Yb diagram for the studied rocks; magenta area includes the samples of spatter cones and the lava related to the tuff ring structures, pink area corresponds to the long lava flows (Las Cortaderas and Laguna Valerio). Black circles along the melting trajectories represent the percentage of melting for spinel- and garnet-peridotite sources, respectively. Basaltic samples of northern *plateau* stage (light grey shaded field), Apas Volcanic Complex (light red shaded area), Barril Niyeu Volcanic Complex (light brown shaded area) and Cerro Corona (yellow area) are also plotted for comparison (data from Remesal *et al.*, 2018, 2012, 2004; Maro & Remesal, 2012; Kay *et al.*, 2007).

the effects of olivine fractionation. The obtained data were employed to assess the melting conditions by means of the equation of Wood (2004). The compositional dependency between pressure and total alkali content of a melt in equilibrium with olivine, orthopyroxene and clinopyroxene, is described by the equation (Wood, 2004):

$$P \text{ GPa} = (\text{MgO} - 11,14 + 1,262 * \text{Alk}) / (2,763 + 0,0945 * \text{Alk})$$

where P is the pressure in GPa, Alk is the weight % of total alkalis ( $\text{Na}_2\text{O} + \text{K}_2\text{O}$ ) in the melt, and MgO is the weight % of MgO in the melt. The equation has an assumed uncertainty of  $\pm 1\%$  and an approximate error of  $\pm 0.33$  GPa. Application of the equation yields an estimation of the melting pressure that is slightly higher for the alkaline basaltic lavas of LC and LV ( $\sim 3.3 \pm 0.33$  GPa;  $\sim 120$  km depth) than for the transitional basalts of the spatter cones and those lavas related to the Tr structure ( $\sim 2.9\text{-}3 \pm 0.33$  GPa;  $\sim 100$  km depth) although the differences are within the uncertainty of the method.

These indicate that melting occurred in the garnet stability field consistent with the trace element data, e.g. high  $\text{Sm}/\text{Yb}_N$  ( $\sim 4\text{-}6$ ). Most of the erupted magmas have segregation depths  $> 100$  km. Since the present thickness of the lithosphere underneath the SCMP is about 60-80 km (Tassara *et al.*, 2006), the source region of the Las Lomadas mafic magmas lay in the asthenospheric mantle

In this connection, the mantle source can also be identified using HFSE/LREE ratios, e.g. Nb/La (Smith *et al.*, 1999): low ratios ( $< 1$ ) suggest a lithospheric origin whereas high ratios indicate an asthenospheric mantle source. The LL lavas have Nb/La ratios between 0.92-1.155 suggesting an OIB-like asthenospheric mantle source although they are lower than average OIB (1.3, Sun & McDonogh, 1995).

#### **Nature of the source, contamination**

Basaltic magmas affected by crustal contamination have La/Nb ratios  $> 1.5$ , La/Ta  $> 22$ , and  $\text{K}/\text{P} > 7$  (e.g. Hart *et al.* 1989). The Las Lomadas rocks have low values of such elemental

ratios ( $\text{La/Nb}=0.85\text{-}1.08$ ;  $\text{La/Ta}=13.68\text{-}17.31$ ;  $\text{K/P}=2.34\text{-}5.94$ , only one sample of LC has  $\text{K/P}$  7.09) which suggest that the magmas would have experienced little or no crustal contamination.

To better understand the characteristics of the source of Las Lomadas magmatism, samples were plotted in the  $\text{Ta/Yb}$  vs.  $\text{Th/Yb}$  diagram (Figure 9), along with other basaltic products of the Somún Curá Formation (northern areas), and ASSCVC, Apas and Barril Niyeu post-*plateau* volcanic complexes. To minimize the effects of fractional crystallization, as well as those of crustal contamination, we considered only basaltic samples from the literature (i.e.:  $\text{SiO}_2 < 54$  wt% and  $\text{MgO} > 3$  wt%). In Figure 9 magmas derived from mid-plate or passive margins lie within or very close to the “Mantle Array” field, with almost constant  $\text{Th/Ta}$  ratios. In contrast, rocks derived from sources modified by subduc-

tion-related metasomatism should retain Th enrichment relative to Ta and Yb (Pearce, 1982) and an upward shift, with higher  $\text{Th/Yb}$  values, for a given  $\text{Ta/Yb}$  ratio, e.g. pointing towards the Global Subducted Sediments (GloSS) field.

Samples from Las Lomadas area plot well within the mantle array, with a time progressive trend towards more enriched compositions. Basalts from neighboring Cerro Corona lie also within the mantle array but displaced towards relatively more depleted compositions. The field of Barril Niyeu basalts stretches in the mantle array partially overlapping the former groups. The *plateau* Somun Curá basalts, in turn, display larger variations between the OIB, E-MORB poles and GLOSS poles, indicating the acquisition of a subduction-related signature during their genesis.

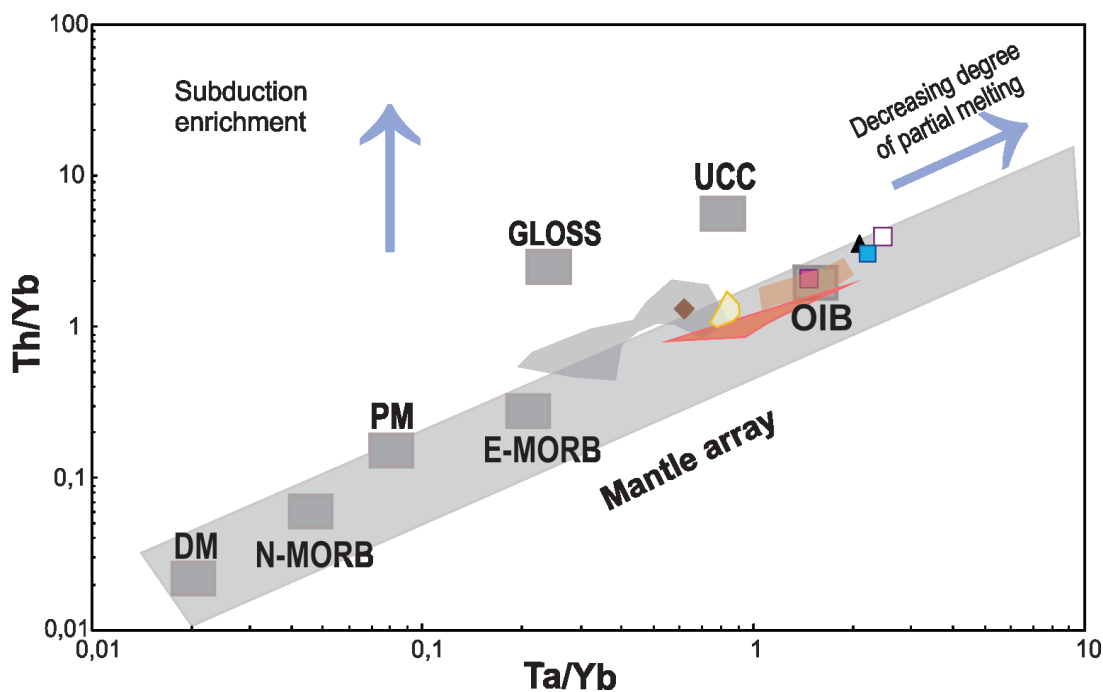


Fig. 9.  $\text{Th/Yb}$  vs.  $\text{Ta/Yb}$  diagram (after Pearce, 1983) for the samples of Las Lomadas area (symbols as in figure 4). Basaltic samples of northern *plateau* stage (light grey shaded field), Apas Volcanic Complex (light red shaded area), Barril Niyeu Volcanic Complex (light brown shaded area) and Cerro Corona (yellow shaded area) are also plotted for comparison (data from Remesal *et al.*, 2018, 2012, 2004; Maro and Remesal, 2012; Kay *et al.*, 2007). DMM=Depleted MORB Mantle (values from Workman and Hart, 2005); N-MORB=Normal MORB, PM=Primitive Mantle, EMORB= Enriched MORB and OIB=Oceanic Island Basalts (values from Sun and McDonough, 1989); UCC=Upper Continental Crust (values from Taylor and McLennan, 1985); GloSS= Global Subducted Oceanic Sediments (values from Plank and Langmuir, 1998). Arrows represent increasing degrees of partial melting and fluid release by the slab.

## ACKNOWLEDGMENTS

We acknowledge the financial support provided by the UBACyT project 20020170100554BA, as well as the SEGEMAR support during field work. Valuable criticisms of an anonymous reviewer helped to improve original manuscript.

## REFERENCES

- Ardolino, A., Franchi, M., Remesal, M. & Salani, F. 2008. La Meseta de Somún Curá: los sonidos de la piedra. En: Ardolino, A. y Lema, H. (eds.), Sitios de Interés Geológico. Anales 46. ISSN 0328-2325.
- Ardolino, A.A. 1981. El vulcanismo cenozoico del borde suroriental de la Meseta de Somuncurá, provincia del Chubut. 8º Congreso Geológico Argentino, Actas 3: 7-23, San Luis.
- Ardolino, A.A & Franchi, M. 1996. Hoja Geológica 4366-1, Telsen: Dirección Nacional del Servicio Geológico, Subsecretaría de Minería de la Nación, Boletín 215,1- 110.
- Cas, R. & Wright, J. 1987. Volcanic successions: modern and ancient. Kluwer, New York.
- Cerrodo, M. E. & Remesal, M. B. 2001. Microestructuras en xenolitos de basaltos postplateau. Meseta de Somún Curá. Provincia de Río Negro. Asociación Geológica Argentina. Serie D: Publicación Especial Nº 5: 65-68
- Cicciarelli, M. 1990. Análisis Estructural del Sector Oriental del Macizo Nordpatagónico y su significado metalogénico. PhD Thesis 555, Facultad de Ciencias Naturales y Museo, 152 p., La Plata
- Corbella, H. 1974. Contribución al conocimiento geológico de la Alta Sierra de Somún Curá, Macizo Nordpatagónico, Provincia de Río Negro, República Argentina. Revista de la Asociación Geológica Argentina 29(2): 155-190
- Corbella, H. 1985. Foiditas noseánicas y otras vulcanitas básicas en la Alta Sierra de Somún Curá, Patagonia Extrandina, Argentina. IV Congreso Geológico Chileno. Actas, 4:89-107, Antofagasta
- Cortés, J.M. 1987. Descripción geológica de la Hoja 42h, Puerto Lobos, provincia del Chubut. Dirección Nacional de Minería y Geología, Boletín 97. 68 p., Buenos Aires.
- Franchi, M., Ardolino A.A. & Remesal, M. 2001. Hoja Geológica N°4166- III, Cona Niyeu. Provincia de Río Negro. Instituto de Geología y Recursos Minerales, Servicio Geológico Minero Argentino. Boletín 262: 1-114, Buenos Aires
- Franchi, M., Haller, M., Lapido, O., Page, R. & Yllañez, E., 1977. Tectónica de la vertiente suroriental del Macizo Nordpatagónico, Servicio Geológico y Minero Argentino, Instituto de Geología y Recursos Minerales, (inédito). Buenos Aires.
- Hart, W. K., Wolde, G. C., Walter, R. C. & Mertzman, S.A., 1989. Basaltic volcanism in Ethiopia: constraints on continental rifting and mantle interactions. Journal of Geophysical Research 94, 7731-7748.
- Kay, S., Ardolino, A., Gorring, M. & Ramos, V. 2007. The Somuncura Large Igneous Province in Patagonia: Interaction of a Transient Mantle Thermal Anomaly with a Subducting Slab. Journal of Petrology 48: 43-77.
- Kinzler, R.J., 1997. Melting of mantle peridotite at pressure approaching the spinel to garnet transition: application to mid-ocean ridge basalt petrogenesis. J. Geophys. Res. 102 (B1), 853-874.
- Lapido, O & Page, R. 1979. Relaciones estratigráficas y estructura del bajo de la Tierra Colorada. Provincia del Chubut. Actas del 7º Congreso Geológico Argentino, 1:299-313. Buenos Aires
- Le Maitre, R.W. (Ed.), 2002. *Igneous Rocks. A Classification and Glossary of Terms*. Cambridge University Press, Cambridge, p. 236.
- Linares, E. 1979. Catálogo de edades radimétricas determinadas para la República Argentina III. Años 1977-1978. Asociación Geológica Argentina. Publicación especial, Serie B (Didáctica y Complementaria), 6. Buenos Aires.
- Maro, G. & Remesal, M. B. 2012. El vulcanismo bimodal del volcán Cerro Corona, Alta Sierra de Somuncurá, provincia de Río Negro. Revista de la Asociación Geológica Argentina, 69 (1): 142 - 151.
- McDonough, W.F. & Sun, S.-S. 1995. Composition of the Earth. Chemical Geology 120: 223-253
- McDonough, W. F. & Frey, F.A., 1989. Rare earth elements in upper mantle rocks. Rev. Mineral. Geochim. 21 (1), 100-145.
- McKenzie, D.P. & O'Nions, R.K., 1991. Partial melt distributions from inversion of rare earth element concentrations. J. Petrol. 32, 1027-1091.
- Noe-Nygaard, A. 1968. On extrusion forms in plateau basalts. Shield volcanoes of 'Scutulium' type. Science in Iceland Anniversary Volume, 10-13. Societas Scientiarum Islandica, Reykjavik
- Plank, T. & Langmuir, C. H. 1998. The chemical composition of subducting sediment and its consequences for the crust and mantle. Chemical Geology, 145(3-4), 325-394
- Pearce, J.A., 1983, Role of the sub-continental lithosphere in magma genesis at active continental margins: p. 230-249 in, Hawkesworth, C.J. and Norry, M.J., eds., Continental Basalts and Mantle Xenoliths, Shiva Publishing Ltd., Cambridge, Mass., 272 p.
- Remesal, M. B, Salani, F. M. & Santos, J. O. 2018a. Alta Sierra de Somún Curá: the youngest volcanic complex of Somún Curá Magmatic Province. Bolivia. La Paz. Libro Resúmenes. 11 South American Symposium on Isotope Geology.
- Remesal, M. B., Cordenons, P. D., Alric, V., & Cerredo, M. E. 2018b. Basaltos del norte de la Meseta de Somún Curá. Provincia de Río Negro. Revista de la Asociación Geológica Argentina. 75 (3): 396-408
- Remesal, M., Parica, C. & Cerredo, M. E. 2017. The Alta Sierra Volcanic Complex, The youngest expression of Somun Cura magmatism. North Patagonia. Argentina. 24<sup>th</sup> Colloquium on Latinamerican Earth Sciences, Libro de resúmenes, 54, Heidelberg, Alemania

- Remesal, M., Cerredo, M. E., Cordenons, P. D. & Salani, F. M. 2016a. The Alta Sierra de Somún Curá Volcanic Complex, characterization of its basaltic components 11 E-ICES, Actas: 84, Malargüe, Argentina
- Remesal, M. B., Cerredo, M.E.; Cordenons, P. D. & Salani, F. M. 2016b. Low-Ca pyroxene reaction coronas in the basalts of Alta Sierra de Somún Cura Volcanic Complex. North Patagonia. *Acta Geológica Lilloana*, 28 (1): 287-292, Special Issue XII Min-Met
- Remesal, M. B., Salani, F. M. & Cerredo, M. E. 2012. Petrología del complejo volcánico Barril Niyeu (Mioceno inferior), Patagonia Argentina, *Revista Mexicana de Ciencias Geológicas*, 29,(2): 463-477
- Remesal, M., Salani, F.M., Massaferro, G.I. & Cerredo, M.E. 2004. Estratigrafía y petrología del sector nor-este de sierra de Apas. Provincia del Chubut, *Revista de la Asociación Geológica Argentina*, (59)4: 578-590.
- Salani, F.M., Remesal, M.B. & Santos, J.O. 2019. Nuevas edades U-Pb SHRIMP del Complejo Volcánico Agua de la Piedra, Provincia Magmatica Somun Cura, Patagonia, Argentina. *Revista Mexicana De Ciencias Geológicas*. In press
- Shaw, C.S.J., Thibault, I., Edgar, A. D. & Lloyd, F. E. 1998. Mechanisms of orthopyroxene dissolution in silica-undersaturated melts at 1 atmosphere and implications for the origin of silica-rich glass in mantle xenoliths, *Contributions to Mineralogy and Petrology*, 132: 354-370.
- Shaw, C.S.J. 1999. Dissolution of orthopyroxene in basaltic magma between 0.4 and 2 GPa: further implications for the origin of Si-rich alkaline glass inclusions in mantle xenoliths, *Contributions to Mineralogy and Petrology*, 135: 114-132.
- Smith, E.I., Sánchez, A., Walker, J.D. & Wang, K., 1999. Geochemistry of mafic magmas in the Hurricane Volcanic Field, Utah: implications for small- and large scale chemical variability of the lithospheric mantle. *Journal of Geology* 107, 433-448.
- Stronck, N.A. & Schmincke, H.U. 2001. Evolution of Palagonite: Crystallization, chemical changes, and element budget. *Geochemistry, Geophysics, Geosystems* 2(7), 1017, doi: 10.1029/2000GC000102.
- Summer, J.M. 1998. Formation of clastogenic lava flows during fissure eruption and scoria cone collapse: the 1986 eruption of Izu-Oshima Volcano, eastern Japan. *Bull Volcanol*: 60:195-212.
- Sun, S.S. & McDonough, W.F., 1989. Chemical and isotopic systematics of oceanic basalts: implications for mantle composition and processes. In: Saunders, A.D., Norry, M.J. Eds. *Magmatism in Ocean Basins*. Geol. Soc. Spec. Publ., London, pp. 313-345.
- Tassara, A., Götze, H.J., Schmidt, S. & Hackney, R. 2006. Three-dimensional density model of the Nazca plate and the Andean continental margin, *J. Geophys. Res.*, 111, B09404, doi:10.1029/2005JB003976.
- Taylor, S.R. & McLennan, S.M. 1985. *The Continental Crust; Its composition and evolution; an examination of the geochemical record preserved in sedimentary rocks*. Blackwell, Oxford. 312.
- Valentine, G.A. & Connor, C.B., 2015. Basaltic volcanic fields. In: Sigurdsson, H. (Ed.), *The Encyclopedia of Volcanoes*, second ed. Elsevier:pp. 423-439 <http://dx.doi.org/10.1016/B978-0-12-385938-9.00023-7>.
- Walker, G.P.L. 2000. Basaltic volcanoes and volcanic systems. *Encyclopedia of Volcanoes*: 283-289
- Walter, M.J. 1998. Melting of garnet peridotite and the origin of komatiite and depleted lithosphere. *J. Petrol.* 39, 29-60.
- Wood, B.J. 2004. Melting of fertile peridotite with variable amounts of H<sub>2</sub>O. *Geophysical Monograph* 150, 69-80.
- Workman, R.K. & Hart, S.R. 2005. Major and trace element composition of the depleted MORB mantle (DMM). *Earth and Planetary Science Letters* 231: 53-72.

Doi: 10.22179/REVMACN.21.635

Recibido: 25-IV-2019

Aceptado: 31-X-2019